DOI: 10.1109/ACCESS.2018.2878146

IEEE Access
Multidisciplinary | Rapid Review | Open Access Journal

Received September 28, 2018, accepted October 15, 2018, date of publication October 30, 2018,
date of current version November 30, 2018.

Digital Object Identifier 10.1109/ACCESS.2018.2878146

Methodology for the Electromagnetic Design of the Axial-Flux C-Core Switched Reluctance Generator

VANESSA SIQUEIRA DE CASTRO TEIXEIRA[1], (Member, IEEE), TÁRCIO ANDRÉ DOS SANTOS BARROS[2], (Member, IEEE), ADSON BEZERRA MOREIRA[1], (Member, IEEE), AND ERNESTO RUPPERT FILHO[3], (Member, IEEE)

[1]Department of Electrical Engineering, Federal University of Ceará, Sobral 62010-560, Brazil
[2]Faculty of Mechanical Engineering, University of Campinas, Campinas 13083-740, Brazil
[3]Faculty of Electrical and Computer Engineering, University of Campinas, Campinas 13083-740, Brazil

Corresponding author: Tárcio André Dos Santos Barros (tarcioandre@hotmail.com)

This work was supported by the São Paulo Research Foundation, FAPESP, under Grant numbers 2017/21640-9 and 15/03248-9.

ABSTRACT The main contribution of this paper is to present a methodology proposal for the electromagnetic design of the axial-flux switched reluctance generator with C core (C-SRG). The proposed methodology focuses on different aspects. First, initial C-core dimensions are obtained from analytic equations and design considerations from the traditional switched reluctance machines. Then, a 2-D finite-element method (FEM) model is used to determine the final constructive parameters of the C-SRG coupled with an iterative optimization process. From the proposed design methodology, a C-core prototype of the generator was built, and the static results were obtained. The C-SRG operational analysis compares the experimental results to the simulations results, which uses a model based on FEM that well represents the nonlinearities of the system. The simulated and experimental results attested the viability and efficiency of the proposed methodology to design the C-SRG for wind power generation.

INDEX TERMS Axial flux, electromagnetic design, finite element method, switched reluctance generator.

I. INTRODUCTION

Switched reluctance machines (SRM) have been gaining ground in research applied to systems requiring high power density, simplicity of construction and low manufacturing costs. These machines have been the subject of studies in the field of electric vehicles and wind power generation, mostly due to the absence of permanent magnetic elements and the presence of coils only in the stator [1]. Thus, these machines have a lighter rotor which, coupled with their intrinsically switched nature (which necessarily requires the presence of an electronic converter for its operation), making them compatible with and attractive for applications in wind power generation [2].

The switched reluctance generator (SRG) is considered a competitive alternative to traditional machines used in wind power generation for small and medium power requirement, because of its operating characteristics, which allow it to function in a wide range of speed at high performance levels [3]. The use of the SRG for wind power systems has been addressed in several studies in the last decade [4]–[6]. Although other topologies have been studied [7], [8], there are few studies that address the application and design of axial flux switched generators for wind power generation.

The main studies exploit procedures for switched motor design. For example, a novel segmented rotor SRM (SSRM) is proposed in [9]. This research shows that the proposed topology has less mutual inductance between phases that the capacity of operating with the fault under phase failure condition is superior to that in the conventional SRM. Besides, a comprehensive study of the structure and electromagnetic characteristics of the SSRM are presented in [10]. Thus, there is a gap regarding the procedures for the electromagnetic design of axial switched reluctance generators, particularly for applications in variable speed generation.

Prominent among the new topologies studied is the Axial-Flux Switched Reluctance Generator with C Core. The C-SRG has as its main feature a modular stator composed of multiple C-shaped cores that are mutually independent. Studies of C-SRG in wind power applications have been carried out in [11]–[14]. Reference [11] presents the design

of the asymmetric half bridge converter for C-SRG and proposes a power control method adjusted for wind power generation systems. Reference [12] describes the operation steps of C-SRG and shows the equivalent magnetic circuit models for the aligned and unaligned positions like that developed by [15] in radial flux reluctance motors. Although [12] addresses some design considerations, it does not detail procedures for calculating motor dimensions. The magnetization process of the SRG with C core is analyzed in [14] and [15]. The high inductance in the windings of reluctance generators limits the excitation level of the magnetic field and prevents magnetization from being rapidly established, compromising power output limits in certain operating conditions. In [14], it is proposed the use of an auxiliary winding to solve this excitation problem and an analysis of this auxiliary winding proposed it is shown in [15], using a computational dynamic model.

In this research, it is described the design methodology, as well as the optimization process of the magnetic core. Firstly, the dimensions of an initial design are calculated. and then an optimization technique is used associated with the two-dimensional finite element method (FEM-2D) to obtain the final dimensions of the magnetic core and windings. After, a two-dimensional finite element method (FEM-2D) model is used to optimize the constructive parameters. The FEM-2D was chosen due to the less computational effort during the optimization process when compared to three-dimensional finite element method (FEM-3D) model. However, it was necessary to include correction factors to calculate the inductances of the C-SRG model.

This paper makes several contributions to the literature. First, it presents a comprehensive framework for the electromagnetic design of the C core switched reluctance generator. Second, the C-SRG is a non-conventional type of the switched reluctance generator and most research focuses on the traditional structure (radial flux SRG), so this paper supplements the literature, addressing this subject poorly investigated. Finally, it's realized an analysis distinct of other paper [11]–[14], presenting a comparative study between the experimental results and the simulation results obtained from two different models (one based on finite element method and the other on the generator's magnetization curves) that well represent the system's nonlinearities.

II. C-CORE: SWITCHED RELUCTANCE GENERATOR

A. A C-SRG STRUCTURE

The axial flux switched reluctance generator has high power density and simplicity of construction, maintenance and repair. Its structure with modular and independent cores, Fig. 1(a), allows each C-core to be built and transported separately for maintenance.

On the constructive aspect, the mainly difference between this topology and the SRG is that the C-SRG has both the characteristics of a linear and a rotational machine, Fig. 1(b). The rotor is composed of magnetic material blocks attached

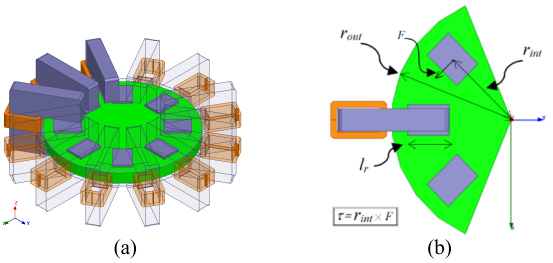

FIGURE 1. C-SRG Structure: (a) three-dimensional view; (b) top view.

to a disk-shaped structure (of low magnetic permeability), solely for support. This topology allows the existence of spare C-cores ready for installation in the event of damaged windings or material fatigue.

The C-SRG has short, unidirectional and independent magnetic flux paths. As shown in [15] and [16], the core losses are direct proportional to the frequency. The flux density waveforms in several segments of the stator and rotor (poles and back iron) vary also with the frequency. For segments in which the flux density is unidirectional, the ripples in flux density waveform increase the core losses. For segments in which the flux density is bidirectional the core losses are still higher. Thus, due the unidirectional magnetic flux paths, the C-SRG has lower core losses when compared to the radial SRG.

On the design aspect, the C-SRG has a low rotor inertia due the possibility of the rotor disc is manufactured with a light material. In addition, the C-SRG presents the advantage of allowing the rise of the electromagnetic torque without changing the magnetic flux paths [17]. As the flux path is independent of the rotor radius, as shown in Fig. 1(b), it is possible to increase the rotor radius without affecting the magnetic circuit.

B. OPERATION PRINCIPLE OF THE C-SRG

The operating principle of C-SRG is based on the variation of the magnetic circuit reluctance during rotor movement, due to the double salient generator poles. The ideal characteristic of the C-SRG inductance curve is shown in Fig. 2. It is noted that inductance is a function of rotor position.

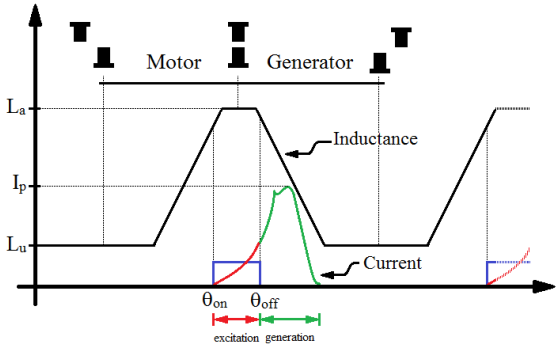

FIGURE 2. Inductance profile and operating modes.

Fig. 2 also features the operating modes of C-SRG: excitation and generation. In the excitation mode, the stator's magnetic core is magnetized by applying a current to the phase winding. In this mode, magnetic energy is stored in the core. In the generation mode, the magnetic energy stored in the previous mode is added to the mechanical torque at the shaft of the motor deriving from the primary motor and transferred to the load [18].

C. OUTPUT EQUATIONS: VOLTAGE AND ELECTRIC POWER

The C-SRG output electric power (P_{ele}) is calculated by (1):

$$P_{ele} = \pi \cdot k_e \cdot k_d \cdot A_s \cdot \omega_{rot} \cdot B \cdot l_r \cdot r_{int}^2 \cdot (1 - L_u/L_a), oxp$$

where k_e is the efficiency factor, k_d is the duty cycle, A_s is the specific electric loading, ω_{rot} is the rotor speed in rad/s, B is the stator pole flux density, l_r is the rotor pole stack length, r_{int} is the inner radius, L_u and L_a are the inductance in the unaligned and aligned position respectively.

$$P_{ele} = \pi \cdot k_e \cdot k_d \cdot A_s \cdot \omega_{rot} \cdot B \cdot l_r \cdot r_{int}^2 \cdot (1 - L_u/L_a), \quad (1)$$

where k_e is the efficiency factor, k_d is the duty cycle, A_s is the specific electric loading, ω_{rot} is the rotor speed in rad/s, B is the stator pole flux density, l_r is the rotor pole stack length, r_{int} is the inner radius, L_u and L_a are the inductance in the unaligned and aligned position respectively.

The variable l_r is a submultiple of the inner radius according to [15]. In this research, l_r is equal to the stator pole width. The efficiency factor k_e is related to the electromechanical energy conversion and it is in a range from 0.8 to 0.93 [17].

The duty cycle, k_d, represents the motor operating cycle and is defined by (2):

$$k_d = (\theta_i \cdot m \cdot N_{ro})/(2 \cdot \pi) \quad (2)$$

where θ_i is phase current conduction angle, m is the number of generator phases and N_{ro} is the number of rotor poles.

The specific electric loading, A_s, is the linear current density along the air gap and can be calculated by means of (3). In general, A_s lies in a range from 20,000 to 90,000 ampere-turns/meters [19].

$$A_s = (2 \cdot N_{turn} \cdot m' \cdot n' \cdot I)/(\pi \cdot D), \quad (3)$$

where N_{turn} is the number of turns per phase, I_p is the peak phase current, m' is the number of simultaneous conducting phases, n' is the number of active poles per phase and D is the rotor inner diameter ($D = 2 \cdot r_{int}$).

The voltage per phase is determined by (4):

$$v = R \cdot i + d\lambda(i, \theta)/dt, \quad (4)$$

where v is the instantaneous winding voltage, R is the winding resistance, i the instantaneous winding current, θ is the rotor position, λ is the flux linkage and t is the time.

Disregarding the resistance R and assuming a constant phase current during the phase conduction time, equation (4) can be simplified to (5):

$$V = I(L_a - L_u)/\Delta t, \quad (5)$$

where V and Δt are the media phase voltage and misalignment poles time respectively.

III. C - SRG DESIGN

The C-SRG design steps are shown in Fig. 3. The proposed methodology involves obtaining the final dimensions of the magnetic core and the coil winding by an initial design (pre-project) calculated from analytical equation. Next, the final dimensions are determinate applying a multi-objective optimization technique.

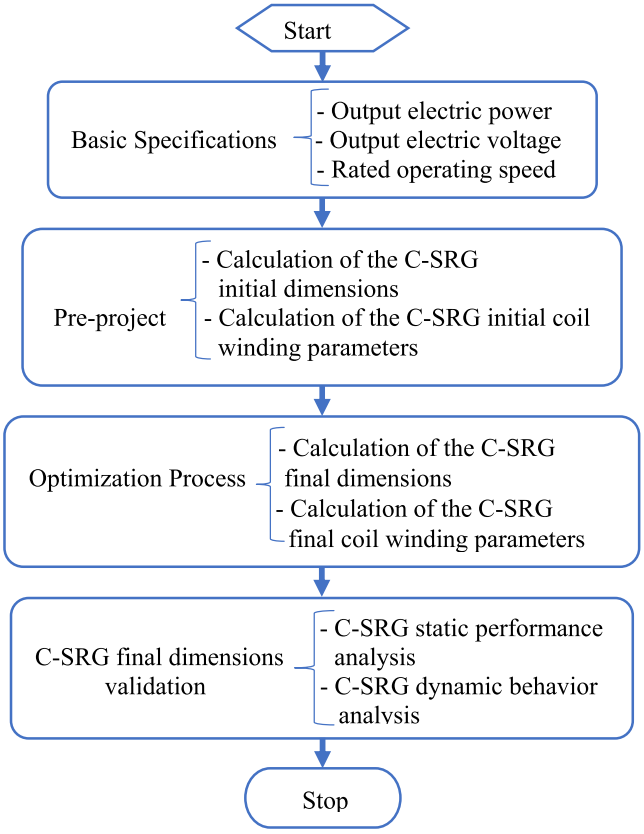

FIGURE 3. Proposed C-SRG design steps.

Although the dimensions of the initial design may be chosen arbitrarily, having initial parameters that meet, albeit partially, the design specification is a good starting point for optimization process, as it speeds up the search process.

A. INITIAL DIMENSIONS OF C-SRG

The design of the C-SRG magnetic core is determined from the generator's output equations and basic specifications such as: rated power, output voltage and rated operating speed. In this research, a C-SRG is designed with electric power and output voltage of 1500W and 180V, respectively, for the rated speed equal to 1500rpm.

Following the steps presented in the Fig. 3, it is necessary to select the geometry of the C-SRG, calculate the dimensions of the magnetic core and determine the stator coil design. These parameters have been documented in the literature for radial

flux reluctance motors. The same procedures may be adapted for the C-SRG.

1) PHASES NUMBER

The phase number is related to the start-up of the machine and ability to operate in two directions of rotation. These requirements can be neglected since the machine is operating in generation mode [1] and the C-SRG can performs with only one phase. However, reluctance generators with a large number of phases are more reliable because they can continue operating for a while in the event of phase loss. For the C-SRG design, it is adopted the phases number equal to three.

2) POLES NUMBER

There are different topologies that can be adopted for the numbers of poles. In general, it is adopted a regular structure with stator pole number (N_{es}) higher than rotor pole number (N_{ro}). Recent research over the use of higher number of rotor poles instead of stator poles number were covered in [20]–[22]. Reference [20], for example, shows that adopting $N_{ro} > N_{es}$, it has the advantage to increasing the specific torque and efficiency, but only at lower current density. In this research, the design of the C-SRG adopted a regular three phases structure with $N_{es} > N_{ro}$.

The multiplicity is defined as the number of pole pairs active simultaneously. One of the effects of the multiplicity is related to the vibration and acoustic noise in reluctance machine [23]. Increasing the multiplicity, in general, reduces the vibration and acoustic noise caused by the electromagnetic radial force produced by excitation. However, this cannot be considered a substantial advantage for a regular C-SRG, since radial force produced by excitation is much smaller than tangential force produced as it will be indicated in the results section.

A significant factor related to the rotor pole number (and to the multiplicity) is the stator frequency for phase or switching frequency, f_s (6):

$$f_s = (\omega_{rot} \cdot N_{ro})/(2 \cdot \pi). \tag{6}$$

Increasing the f_s, the commutation torque ripple frequency increases as well, making the filtering system easier. On the other hand, the switching and core losses also increase [13], [16]. Thus, it is suggested doing a cost benefits analysis in accordance to the application. In this design, it is adopted multiplicity equal to 2 (C-SRG 12/8) since the aim is to validate the project methodology.

3) AIR GAP LENGTH

The air gap length has a strong influence on magnetomotive force produced by the magnetic circuit. The smaller the air gap length is, the smaller the current phase required to produce the same quantity of magnetomotive force will be. But, due mechanical limitations, the smallest air gap practical for industrial machines is around 0.2 mm [24]. It is used air gap equal to 0.25 mm in the project of the C-SRG.

4) POLE ARCS

The pole arcs dimensions define the effective zone of electromagnetic torque and can ensure a better use of the inductance curve. According to [25], for a regular machine, the pole arc of the stator (β_{es}) and the pole arc of the rotor (β_{ro}) must meet the following constructive relations: $\beta_{ro} \geq \beta_{es}$ and $(\beta_{ro} + \beta_{es}) \leq (2\pi / N_{ro})$.

A third constructive relation can be defined from the need to reduce the torque ripple. The angular distance between adjacent phase inductances (ε) is defined by (7).

$$\varepsilon = (2 \cdot \pi)/(m \cdot N_{ro}) \tag{7}$$

As indicated in [26], in order to reduce the torque ripple during the commutation, it is necessary the presence of an overlapping angle between the inductance curves adjacent, in other words, $\beta_e \geq \varepsilon$.

Based on these three criteria, the limits of the pole arcs can be defined in a feasible triangle as shown in Fig. 4. The pole arcs of the initial project are chosen arbitrarily in accordance with the feasible triangle limits.

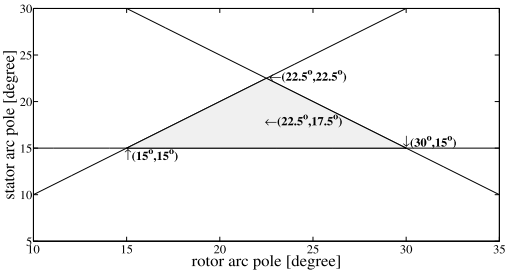

FIGURE 4. Limits of the pole arcs.

5) STATOR AND ROTOR WIDTH

The stator width (l_{es}) and rotor width (l_{ro}) poles are given by (8) and (9):

$$l_{es} = (D/2) \cdot \beta_{es} = r_{int} \cdot \beta_{es} \tag{8}$$

$$l_{ro} = (D/2) \cdot \beta_{ro} = r_{int} \cdot \beta_{ro} \tag{9}$$

6) ROTOR INNER RADIUS

The rotor inner radius, r_{int}, is calculated from the output electric power equation (1). Thus, r_{int} is obtained by (10):

$$r_{int} = ((P_{ele})/(\pi \cdot k_e \cdot k_d \cdot A_s \cdot \omega_{rot} \cdot B \cdot 2 \cdot tan(\beta_{es}/2) \cdot k_2))^{1/3} \tag{10}$$

where $k_2 = (1 - L_u/L_a)$.

The variable k_2 depends on the operating point of the generator. For radial-flux reluctance machines (SRM) at rated point operating, k_2 is generally in the range of 0.65 – 0.75 according to [15]. So, it is assumed k_2= 0.65 in the initial project of the C-SRG. Also, it is adopted B = 1.4 T (knee of the material magnetization curve) and A_s = 40000. These values will be corrected during the optimization process.

7) POLES HEIGHTS

The height of the stator pole (h_{es}) in SRM is related to the coil height as well as the height of the rotor pole (h_{ro}) is related to the bore diameter of the machine. These criteria are not required for the C-SRG since the coil is not located in the pole and the rotor poles are embedded in the rotor disc.

Reference [27] presents that the stator and rotor heights of the SRM are related to the pole spans. These relations are described in (11) and (12). These relations are also applied to estimate the h_{es} and h_{ro} of the C-SRG.

$$h_{es}/(\pi \cdot D/2 \cdot N_{es}) \approx h_{es}/(\pi \cdot r_{int}/N_{es}) \approx (0.7 - 0.8) \tag{11}$$

$$h_{ro}/(\pi \cdot D/2 \cdot N_{ro}) \approx h_{ro}/(\pi \cdot r_{int}/N_{ro}) \approx (0.7 - 0.8) \tag{12}$$

Note that it could be adopted h_{es} =0. However, it is established a value unequal to zero as design criteria in order to direct better the magnetic flux through the air gap. The height of the rotor pole could also be estimated if the slot height (h_{slot}) is known, using $h_{ro} = h_{slot} - 2 \cdot h_{es} - 2 \cdot l_{gap}$.

8) COIL DIMENSIONS: NUMBER OF TURNS AND SLOT DIMENSION

The main issue of the number of turns in conventional electric machines is how to allocate the coils into the stator or rotor slots without exceeding the suitable limit of space and refrigeration. But, the C-SRG has a large space available to allocate the coils [17]. Also, the coils are located on the outer circumference, facilitating the air flow path and the heat exchange with the environment.

The number of turns per phase can be obtained from (3) for a given specific electric load and maximum permissible current on the conductor [15]. Note that the specific electric load depends on the generator cooling system.

The slot length (l_{slot}) depends on the number of turns. It should be checked if the slot area is enough to hold the winding according to the fill factor. In general, the winding fill factor is defined in a range of 0.2 – 0.7 and it is defined as: fill factor = (stator winding area) / (stator slot window area).

9) C-SRG INITIAL PARAMETERS

The dimensions of the initial generator design and the views of the stator core are shown in Fig. 5 and Table 1.

B. OPTIMIZATION AND FINAL DIMENSIONS OF THE C-SRG

The final dimensions of the magnetic C-Core are calculated using an optimization technique. The aim is to obtain a reluctance generator with output electric power between 1.5kW and 2.0kW and induced voltage at the terminal between 90V and 180V. Therefore, there is more than a goal to be achieved, characterizing the problem as multi-objective. Furthermore, the FEM-2D is coupled with the iterative optimization process to better represent the system's nonlinearities.

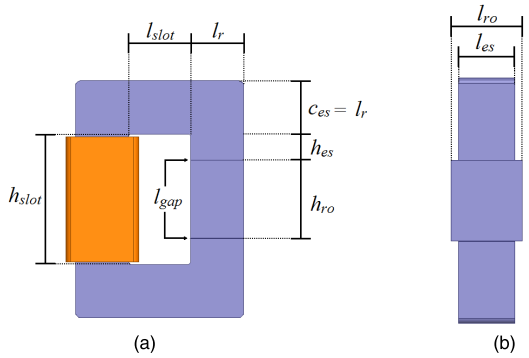

FIGURE 5. C-SRG: Prototype views: (a) front view; (b) side view.

TABLE 1. Initial parameters of the C-SRG.

Parameter	Value	Parameter	Value
Stator poles number (N_{es})	12	Rotor poles number (N_{ro})	8
Rotor internal radius (r_{int})	86 mm	Poles stack length (l_j)	27 mm
Stator pole arc ($_{es}$)	0.308 rad	Rotor arc pole ($_{ro}$)	0.395 rad
Stator pole width (l_{es})	27 mm	Rotor pole width (l_{ro})	35 mm
Stator pole height (h_{es})	16 mm	Rotor pole height (h_{ro})	48 mm
Air gap length (l_{gap})	0.25 mm	C–core rated current (I)	5 A
Slot length (l_{slot})	40 mm	Slot height (h_{slot})	80.5 mm
Number of turns per C-core (N_{turn})	271	Specific electric load (A_s)	20000

The optimization process seeks a solution vector within a four-dimension Euclidean space $[x_1x_2x_3x_4]$ that is the best solution for the vector formed with the objective functions $[f_1(x)f_2(x)]$, also defined within a Euclidean space. It is observed that in multi-objective optimization, there is no single optimal solution, but a set of possible, non-dominated solutions also known as Pareto optimal solutions.

The variables of the solution vector $[x_1x_2x_3x_4]$ are respectively: N_{turn}, r_{int}, β_{es} e β_{ro}. The maximum and minimum values of each variable vector are defined in Table 2.

TABLE 2. Minimum and maximum values for the vector x.

Parameter	N_{turn}	r_{int} (mm)	$_{es}$ (rad)	$_{ro}$ (rad)
Minimum	160	50	0.2618	0.2618
Maximum	800	150	0.39269	0.52359

The optimization technique adopted is the Weighting Method. This method is one of the most common forms of solving multi-objective problems and presents as advantage its simplicity. It reduces the multi-objective function to a single-objective scalar function by assigning different weight values to each objective function, according to (13) and (14):

$$OF(x) = min(w_i \cdot c_i \cdot f_i(x)), \quad i = 1, 2 \tag{13}$$

$$x_3 - x_4 \leq 0 \quad and \; x_3 + x_4 \leq 0.78539. \tag{14}$$

The weights vector is represented by variable w where: $w > 0$ and $||w|| = 1$. Variable c_i is a normalization factor given by (15). Data normalization is necessary to compare the objectives in a same scale during the optimization.

$$c_i = 1/[max(f_i(x)) - min(f_i(x))] \quad (15)$$

The objective functions f_1 and f_2 are respectively the relative squared error of the output electric power (16) and the relative squared error of the output phase voltage, E_{ind}, (17):

$$f_1(x) = ((P_{ele}(x) - P_{rel})/P_{rel})^2, \quad (16)$$
$$f_2(x) = ((E_{ind}(x) - E_{rel})/E_{rel})^2, \quad (17)$$

where P_{rel} is the reference output electric power and E_{rel} is the reference induced voltage.

The multi-objective function (OF) is minimized using a direct search algorithm called Pattern Search in optimization toolbox of the Matlab. This method not require any information about the gradient or derivative of the OF and finds the solution by an interactive process. This method searches a set of points (a new solution vector) around the current point (current solution vector), looking for one where the value of the OF is lower than the value at the current point [28].

At each algorithm iteration, the inductance values in the aligned and unaligned position are determined by FEM-2D. The two-dimensional finite element method was chosen due to its low computational effort compared to FEM-3D. Because of the three-dimensional nature of the magnetic flux distribution in C-SRG, calculating the inductance by FEM-2D is imprecise, especially in the unaligned position. These errors are attributed to the magnetic flux paths present in the dimension which is not considered in FEM-2D.

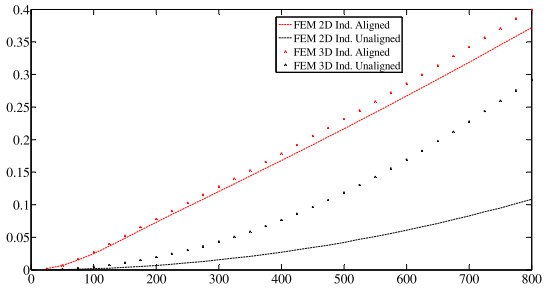

FIGURE 6. C-SRG: Inductance versus turns number.

The Fig. 6 shows the difference between the inductances calculated by the FEM-2D an FEM-3D for the aligned and unaligned rotor position. In the aligned position, the effect of the spreading out of magnetic flux is small because the gaps between the stator and rotor poles are minimums. So, the flux paths that acts in the dimension which is not considered in the FEM-2D are not too relevant.

In contrast, the gap between the stator and rotor poles in the unaligned position is maxima. In this case, the effect of the spreading out of magnetic flux in the three dimensions are relevant. Thus, the FEM-2D presents a considerable error in the inductance calculation relative to the FEM-3D.

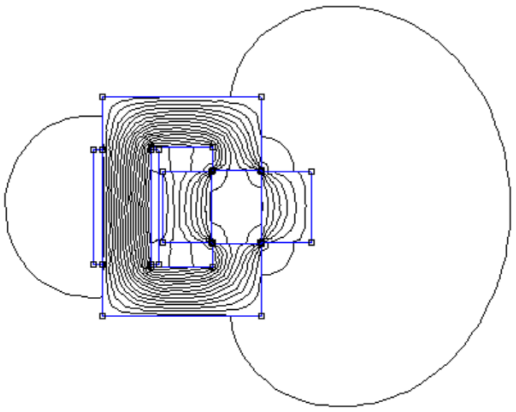

FIGURE 7. FEM-2D model: unaligned position.

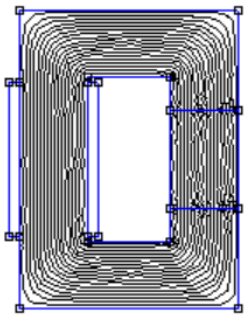

FIGURE 8. FEM-2D model: aligned position.

To reduce this difference, correction factors (k_a and k_u) are determinate and applied in FEM-2D models, as shown in Fig. 7 and Fig. 8, to calculate the inductance in the aligned and unaligned positions. These factors were estimated based on the inductance to the desired position, according to the level of the magnetic material saturation. For a set of points within the search range of the number of turns, the difference is checked between the inductance values calculated by FEM in two and three dimensions. The k_a and k_u factors are calculated from the interpolation of the percent error between these two inductances based on an equivalent turns number to the magnetic saturation of the material as shown in (18) and (19):

$$k_a = 1/(1 - erro_a) = 1/(1 - ((L_{a_3D} - L_{a_2D})/L_{a_3D}))^2, \quad (18)$$
$$k_u = 1/(1 - erro_u) = 1/(1 - ((L_{u_3D} - L_{u_2D})/L_{u_3D})), \quad (19)$$

where $error_a$ and $error_u$ are the inductance percent errors in aligned and unaligned position respectively, L_{a_3D} and L_{u_3D} are the aligned and unaligned inductances calculated by FEM-3D, L_{a_2D} and L_{u_2D} are the aligned and unaligned inductances calculated by FEM-2D.

Applying the weighting method to minimize OF, the Pareto Distribution was determined for the generator, as illustrated in Fig. 8. Following the determination of the Pareto curve, decision-making procedures are necessary to define which one of the optimal design will be adopted.

There are several techniques and algorithms in the literature that perform decision-making. In general, they are related to reducing final design costs and facilitating manufacture. As this design has no commitment between cost and manufacturing, the decision criterion adopted for the prototype was the closest point to the two initial objectives: f_1 and f_2 closest to zero. To this end, a circumference was drawn centered at (0.0).

The optimal point of the Pareto curve closest to the circumference for the C-SRG is shown in Tables 3 and the final dimensions are shown in Table 4.

TABLE 3. Optimization results of the C-SRG.

N_{turn} (ad)	295	β_{es} (rad)	0.377	f_1	0.0048
r_{int} (mm)	84	β_{ro} (rad)	0.377	f_2	0.0049

TABLE 4. Final C-SRG parameters of the C-SRG.

Parameter	Value	Parameter	Value
Stator poles number (N_{es})	12	Rotor poles number (N_{ro})	8
Rotor internal radius (r_{int})	84 mm	Poles stack length (l_r)	33 mm
Stator pole arc (β_{es})	0.377 rad	Rotor arc pole (β_{ro})	0.377 rad
Stator pole width (l_{es})	33 mm	Rotor pole width (l_{ro})	33 mm
Stator pole height (h_{es})	16 mm	Rotor pole height (h_{ro})	47 mm
Air gap length (l_{gap})	0.25 mm	C–core rated current (I)	5 A
Slot length (l_{slot})	40 mm	Slot height (h_{slot})	79.5 mm
Number of turns per C-core (N_{turn})	295	Specific electric load (A_s)	22375

IV. DISCUSSIONS AND RESULTS

Simulations and experimental test were implemented to validate the proposed design methodology and the final dimensions of the C-core generator. Due the limitations in the project financials, only a single C-core was built. However, only a C-Core is sufficient to obtain the static and dynamics results on account of the modular and symmetrical structure of C-SRG.

The static simulations were developed in Maxwell 3D software (Ansys) and the static experimental results were obtained using a data acquisition software developed in the Labview®to extract the data of the oscilloscope via Ethernet.

A. STATIC SIMUTATION RESULTS

The distribution of the magnetic flux density on the fully aligned and unaligned positions of the final design of the C-SRG is shown in Fig. 10(a) and Fig. 10(b). The results of the flux density magnitudes in the stator pole for the aligned and misaligned positions are 1.41T and 0.17 T respectively.

As expected, the field densities in the aligned positions are around 1.4T, i.e., in the knee region of the magnetization curve of the magnetic material, according to Fig. 11.

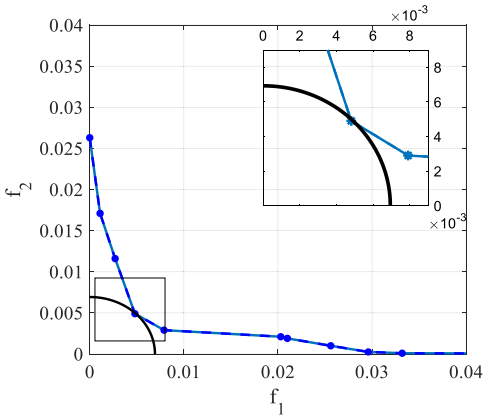

FIGURE 9. Pareto distribution weighting method.

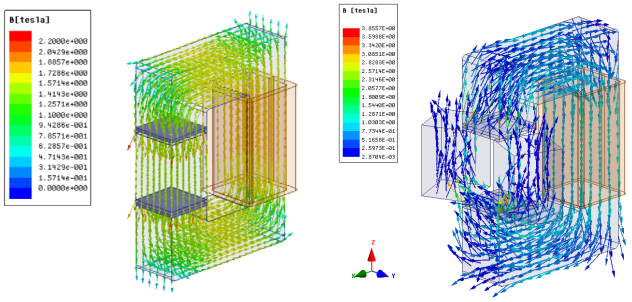

FIGURE 10. Magnetic flux density vector in C-core: (a) aligned position; (b) unaligned position.

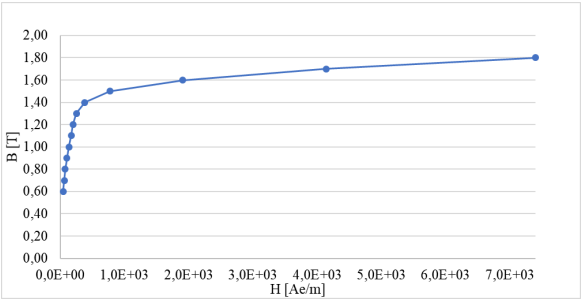

FIGURE 11. Magnetization curve: E 230.

The simulated flux linkage waveforms are shown in Fig. 12. The work per cycle (W_m) done by each C core is obtained by calculating the area between the flux linkage curves in the aligned (0°) and unaligned (22.5°) positions of the poles. The maximum static output electric power (P_{max_sta}) is obtained by (20):

$$P_{max_sta} = ((n' \cdot W_m \cdot m \cdot N_{ro})/2 \cdot \pi) \cdot \omega_{rot} \quad (20)$$

It is observed that this would be the output electric power if the electric current in the windings remained constant and the entire inductance decreasing curve were used during the generation stage. That does not occur during dynamic

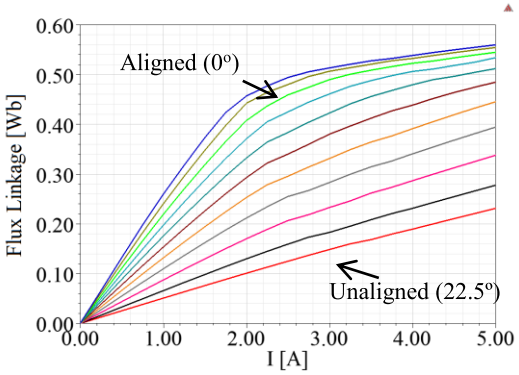

FIGURE 12. FEM-3D flux linkage waveforms.

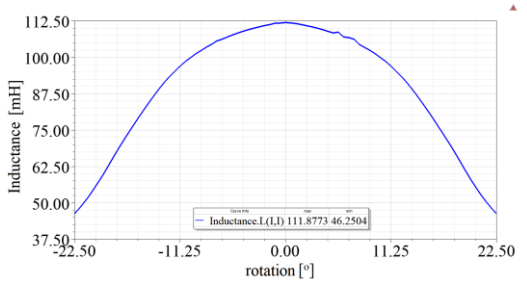

FIGURE 13. Inductance profile -- FEM 3D.

operation. The static power calculated by means of (20) for the C-SRG prototype is equal to 3.50 kW.

Fig. 13 illustrates the inductance profile simulated for the C-SRG designed. The inductance values L_a and L_u are shown in the legend. Applying these values in (5) determines the average induced voltage in each winding. The output electric power for each generator can also be determined by applying in (1) the L_a and L_u values, as well as the other parameters required in the equation shown in Tables 5 and 6. The values obtained for P_{ele} and E_{ind} are 1.65 kW and 136.72 V respectively.

B. EXPERIMENTAL RESULTS

The system (C-Core + Mechanical Base) developed is shown in Fig. 14. The material used to build the C-Core is the silicon steel E 230. The experimental magnetization curves were obtained applying direct procedures measurements, i.e., from measurements of the electric voltage and current in the C-core phase windings.

There are several direct techniques to determine the magnetization curves. The simplest method consists to calculate the magnetic flux from an electric voltage applied in the generator phase winding for different position between the stator and rotor' poles. However, this method will present significant error if the magnetic material operates in the saturation region. So, it is inappropriate for switched reluctance machines since they operate in the saturation region constantly.

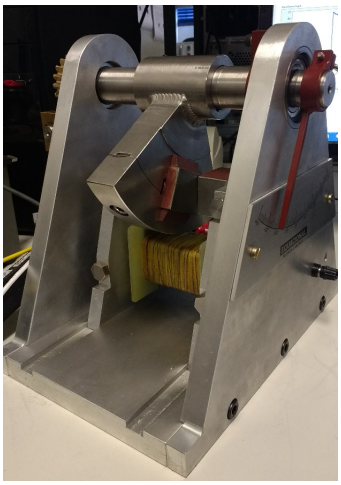

FIGURE 14. C-SRG Prototype: isometric view.

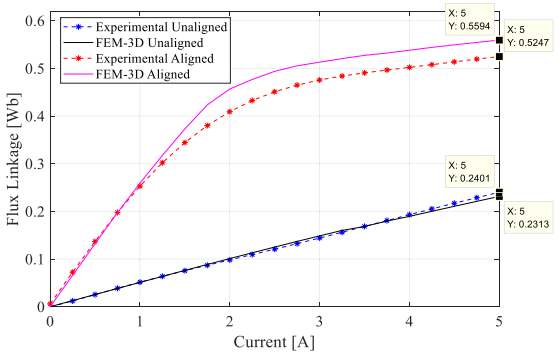

FIGURE 15. Experimental and simulated flux linkage waveforms.

According to [29], the most effective direct method for obtaining the magnetization curves involves applying a voltage step in the C-core phase winding, for different locked rotor positions between the aligned and unaligned region and storing the current (i) and voltage (v) responses. Such as the winding phase resistance is knowing, the magnetic flux is determinate by (21):

$$\varphi(t) = \int (V - R \cdot i)dt \tag{21}$$

where t is the total time of the step.

The experimental test consists in varying (manually) the rotor to the position desired and block the rotor with the mechanical lock. After, a step voltage is applied in the C-Core winding phase and the current and voltage responses are stored. Using a data acquisition software developed in the Labview®to extract the data of the oscilloscope and calculate the magnetic linkage flux, it was obtained the magnetization curves in the aligned and unaligned position and compared to the simulated results according Fig. 15.

The inductance behavior is calculated by the ratio $\lambda = L \cdot i$. Thus, the experimental magnetic flux linkage was divided by the test current and the inductance curve for the rated current was obtained as shown in Fig. 16.

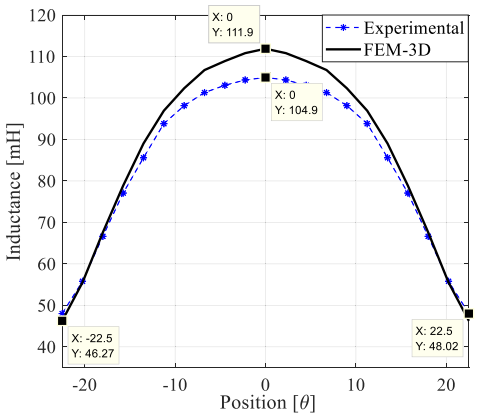

FIGURE 16. Experimental and simulated inductances curves.

TABLE 5. Comparison of the static results.

GRV-C	Inductance		Flux Linkage		Power	
	L_a (mH)	L_u (mH)	λ_a (Wb)	λ_u (Wb)	P_{max_sta} (kW)	P_{ele} (kW)
Experimental	104.9	48.02	0.524	0.240	3.16	1.52
FEM- 3D	111.9	46.27	0.559	0.230	3.50	1.65
FEM 2D (adjusted)	112.2	49.29	0.560	0.246	3.38	1.58

TABLE 6. Errors: inductance and flux linkage.

GRV-C	Inductance		Flux Linkage	
	L_a (mH)	L_u (mH)	λ_a (Wb)	λ_u (Wb)
Experimental	104.9	48.02	0.520	0.240
FEM- 3D	111,9 (6.7%)	46.27 (3.6%)	0.559 (7.5%)	0.230 (4.2%)
FEM 2D (adjusted)	112.2 (6.9%)	49.29 (2.6%)	0.5608 (7.8%)	0.246 (2.5%)

To analyze the experimental results, statics simulations using finite element in two dimensions were also developed allowing to compare the results and validate the design methodology proposed. It was analyzed only the data of the aligned and unaligned position due their relevance on the design methodology.

The comparison of the experimental and simulated results is is detailed in the Table 6, which are: magnetic flux linkage on aligned position (λ_a), magnetic flux linkage on unaligned position (λ_u), inductance on aligned position (L_a), inductance on unaligned position (L_u), maximum static output electric power (P_{max_sta}) and output electric power (P_{ele}). The errors related to the experimental results of each parameters simulated are presented in Table 5 and 6. It is also important to highlight that the maximum static output electric power and output electric power are not measured directly. They are derived from the inductance and magnetic flux linkage measured and from the C core dimensions.

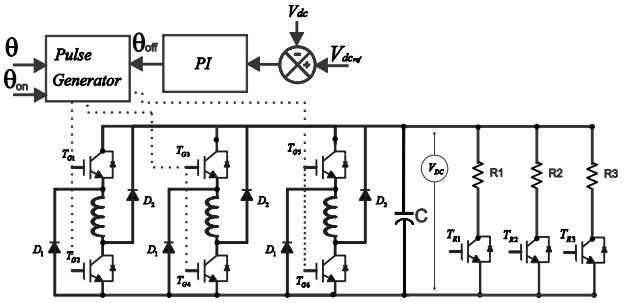

FIGURE 17. C-SRG power electronic converter and drive control system.

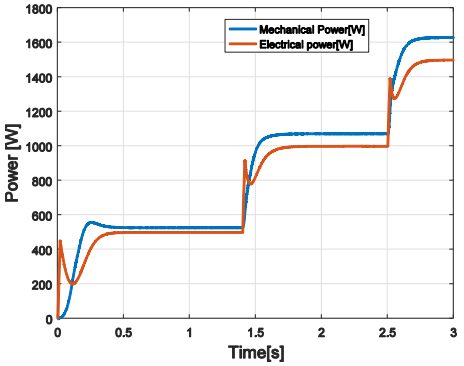

FIGURE 18. Mechanical and output electric power for the Generator 1.

Notes that the errors of the simulations results related to the experimental tests reach a maximum of 10%, That is an acceptable level of error in design of reluctance electric machines [15], consequently, it makes the proposed methodology appropriate for the C-SRG project.

C. DYNAMIC SIMULATION RESULT

The dynamic responses of the generators were determined through simulations developed in Matlab/Simulink software. For each generator, a model was implemented and coupled to a control and drive system – Fig. 17. The C-SRG model is developed based on the magnetization curves of each generator acquired in static tests. The procedures for obtaining these models have been described in [30].

The voltage control system was designed to maintain the voltage on the DC bus constant even after load insertion. It uses an integral proportional compensator that adjusts the turn off angle (θ_{off}) based on the error between the reference voltage and the measured value of the DC bus voltage. The C-SRGs are self-excited, i.e., they do not require another source for magnetization. The initial voltage on the capacitor is 180V.

During the test, three 500W loads are added gradually (R1, R2, R3). The system is initiated with the R1 load connected to the DC bus. The R2 and R3 loads are connected at 1.4s and 2.5s, respectively.

According to Fig. 18, it is observed that the designed C-SRGs generated 1.5kW of power at rated operating speeds. Furthermore, the control system kept the voltage at 180V for three simulated generators following load insertion – Fig. 19.

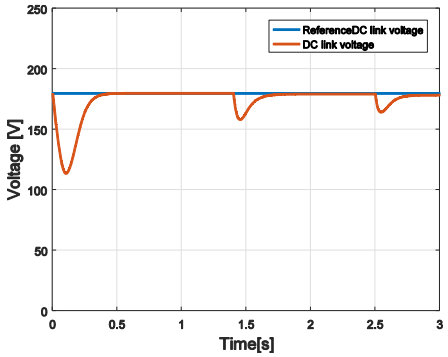

FIGURE 19. DC bus voltage for the three designed C-SRGs.

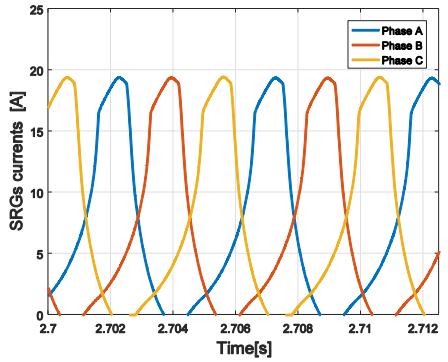

FIGURE 20. SRG currents.

Fig. 20 features the electric currents C-SRG during the period in which the generated power is 1500W. It is noted that in the three designed C-SRGs, the current increases in the generation period, so the exciting factor and, consequently, electric loss are smaller [30].

V. CONCLUSION

The proposed methodology uses an interactive model implemented in the software Matlab® along with Finite Element Method Magnetics (FEMM) to obtaining the generator dimensions. The two-dimension finite element model is used in the design process to reduce computational effort during the optimization process when compared to three-dimensional finite element method. However, it is necessary to include correction factors in the model. Comparing the static simulation results obtained by the FEM–2D model and the FEM-3D model, we conclude that the methodology applied is suitable to obtain the final dimensions of the C-SRG. A prototype of the C-Core was built in order to validate the methodology. The comparison of the static experimental and simulated results attests the viability and efficiency of the proposed methodology to design C-SRG for wind power generation.

REFERENCES

[1] S. Mendez, A. Martinez, W. Millan, C. E. Montano, and F. Perez-Cebolla, "Design, characterization, and validation of a 1-kW AC self-excited switched reluctance generator," *IEEE Trans. Ind. Electron.*, vol. 61, no. 2, pp. 846–855, Feb. 2014.

[2] D. A. Torrey, "Switched reluctance generators and their control," *IEEE Trans. Ind. Electron.*, vol. 49, no. 1, pp. 3–14, Feb. 2002.

[3] T. A. S. Barros, P. J. S. Neto, P. S. N. Filho, A. B. Moreira, and E. Ruppert, "Approach for performance optimization of switched reluctance generator in variable-speed wind generation system," *Renew. Energy*, vol. 97, pp. 114–128, Nov. 2016.

[4] R. Cardenas, W. F. Ray, and G. M. Asher, "Switched reluctance generators for wind energy applications," in *Proc. IEEE PESC*, vol. 1, Jun. 1995, pp. 559–564.

[5] E. A. E. Jebaseeli and D. Susitra, "Performance analysis of various configurations of switched reluctance machine for wind energy applications," in *Proc. Recent Adv. Space Technol. Services Climate Change*, 2010, pp. 419–423.

[6] D.-W. Choi, S.-I. Byun, and Y.-H. Cho, "A study on the maximum power control method of switched reluctance generator for wind turbine," *IEEE Trans. Magn.*, vol. 50, no. 1, Jan. 2014, Art. no. 4003004.

[7] J. F. Pan, C. C. Sun, G.-Z. Cao, and N. C. Cheung, "Design and simulation of a novel planar switched reluctance generator," in *Proc. 4th Int. Conf. Power Electron. Syst. Appl.*, Jun. 2011, pp. 1–3.

[8] J.-H. Oh and B.-I. Kwon, "Design, optimization, and prototyping of a transverse flux-type-switched reluctance generator with an integrated rotor," *IEEE Trans. Energy Convers.*, vol. 31, no. 4, pp. 1521–1529, Dec. 2016.

[9] X. Sun, Z. Xue, S. Han, L. Chen, X. Xu, and Z. Yang, "Comparative study of fault-tolerant performance of a segmented rotor SRM and a conventional SRM," *Bull. Polish Acad. Sci.-Tech. Sci.*, vol. 65, no. 3, pp. 375–381, 2017.

[10] X. Sun, Z. Zhou, L. Chen, Z. Yang, and S. Han, "Performance analysis of segmented rotor switched reluctance motors with three types of winding connections for belt-driven starter generators of hybrid electric vehicles," *Int. J. Comput. Math. Elect. Electron. Eng.*, vol. 37, no. 3, pp. 1258–1270, 2018.

[11] Y. J. Bao, K. W. E. Cheng, X. D. Xue, J. Chan, Z. Zhang, and J. K. Lin, "Research on a novel switched reluctance generator for wind power generation," in *Proc. Power Electron. Syst. Appl. (PESA)*, 2011, pp. 1–6.

[12] X. D. Xue, K. W. E. Cheng, Y. J. Bao, and J. Leung, "Design consideration of C-core switched reluctance generators for wind energy," in *Proc. Power Electron. Syst. Appl. (PESA)*, 2011, pp. 1–6.

[13] X. Liu, K. Park, and Z. Chen, "A novel excitation assistance switched reluctance wind power generator," *IEEE Transaction Magn.*, vol. 50, no. 11, Dec. 2014, Art. no. 8203304.

[14] X. Liu, C. Wang, and Z. Chen, "Characteristics analysis of an excitation assistance switched reluctance wind power generator," *IEEE Trans. Magn.*, vol. 51, no. 11, Nov. 2015, Art. no. 8700404.

[15] K. Ramu, *Switched Reluctance Motor Drives: Modeling, Simulation, Analysis, Design, and Applications*. Boca Raton, FL, USA: CRC Press, 2011.

[16] X. Sun, Y. Shen, S. Wang, G. Lei, Z. Yang, and S. Han, "Core losses analysis of a novel 16/10 segmented rotor switched reluctance BSG motor for HEVs using nonlinear lumped parameter equivalent circuit model," *IEEE/ASME Trans. Mechatronics*, vol. 23, no. 2, pp. 747–757, Apr. 2018.

[17] A. Labak and N. C. Kar, "Designing and prototyping a novel five-phase pancake-shaped axial-flux SRM for electric vehicle application through dynamic FEA incorporating flux-tube modeling," *IEEE Trans. Ind. Appl.*, vol. 49, no. 3, pp. 1276–1288, May/Jun. 2013.

[18] V. S. de Castro Teixeira, E. R. Filho, T. A. D. S. Barros, and A. B. Moreira, "Design, optimization and analysis of the axial C-core switched reluctance generator for wind power application," in *Proc. ICRERA*, 2015, pp. 833–837.

[19] R. Krishnan, M. Abouzeid, and X. Mang, "A design procedure for axial field switched reluctance motors," in *Proc. Conf. Rec. IEEE Ind. Appl. Soc. Annu. Meeting*, vol. 1, Oct. 1990, pp. 241–246.

[20] P. C. Desai, "The novel concept of switched reluctance machines with higher number of rotor poles," Dept. Elect. Comput. Eng., Illinois Inst. Technol., Chicago, IL, USA, Tech. Rep., 2009, p. 245.

[21] S. Smaka, Š. Mašić, N. Hadžimejlić, and M. Ćosović, "Design considerations for novel 8/14 and comparison with conventional 8/6 and 8/10 switched reluctance machines," in *Proc. Symp. Power Electron., Elect. Drives, Automat. Motion*, Sorrento, Italy, 2012, pp. 614–619.

[22] R. Vandana, S. Nikam, and B. G. Fernandes, "Criteria for design of high performance switched reluctance motor," in *Proc. 20th Int. Conf. Electr. Mach. (ICEM)*, Marseille, France, 2012, pp. 129–135.

[23] T. J. E. Miller, *Electronic Control of Switched Reluctance Machines*. Oxford, U.K.: Newnes, 2001.

[24] J. Pyrhonen, T. Jokinen, and V. Hrabovcova, *Design of Rotating Electrical Machines*. Hoboken, NJ, USA: Wiley, 2008.

[25] S.-H. Mao and M.-C. Tsai, "A novel switched reluctance motor with C-core stators," *IEEE Trans. Magn.*, vol. 41, no. 12, pp. 4413–4420, Dec. 2005.
[26] P. Lobato, J. Martin, and A. J. Pires, "A design criteria for torque ripple reduction in switched reluctance generators," in *Proc. Int. Conf. Power Eng., Energy Elect. Drives*, Torremolinos, Spain, 2011, pp. 1–6.
[27] I. Boldea, *Variable Speed Generators*. Boca Raton, FL, USA: CRC Press, 2005.
[28] M. Taktak, K. Omheni, A. Aloui, F. Dammak, and M. Haddar, "Dynamic optimization design of a cylindrical helical spring," *Appl. Acoust.*, vol. 77, pp. 178–183, Mar. 2014.
[29] W. Ding and D. Liang, "A fast analytical model for an integrated switched reluctance starter/generator," *IEEE Trans. Energy Convers.*, vol. 25, no. 4, pp. 948–956, Dec. 2010.
[30] T. A. D. S. Barros, P. J. D. S. Neto, M. V. De Paula, A. B. Moreira, P. S. N. Filho, and E. R. Filho, "Automatic characterization system of switched reluctance machines and nonlinear modeling by interpolation using smoothing splines," *IEEE Access*, vol. 6, pp. 26011–26021, 2018.

VANESSA SIQUEIRA DE CASTRO TEIXEIRA was born in Fortaleza, Brazil. She received the B.S. and M.S. degrees from the Federal University of Ceará, Brazil, in 2004 and 2008, respectively, and the Ph.D. degree from the State University of Campinas, Campinas, Brazil, in 2018, all in electrical engineering. She is currently a Professor of electrical engineering with the Federal University of Ceará at Sobral Campus. Her research interests include energy efficiency, electromagnetic design and modeling of electric machines and innovations in electric machines, and drives systems.

TARCIO ANDRÉ DOS SANTOS BARROS (S'14–M'17) received the bachelor's degree in electrical engineering from the Federal University of Vale do São Francisco, Petrolina, Brazil, in 2010, and the M.S. and Ph.D. degrees from the University of Campinas, Campinas, Brazil, in 2012 and 2015, respectively. From 2016 to 2017, he was a Researcher with the University of Campinas, under the FAPESP Post-Doctoral Program. He is currently a Professor with the University of Campinas. He is involved in the areas of electrical machines, power electronics, and electrical drives. His research interests include machine drives, switched reluctance machines, doubly fed induction generators, and solar energy. He is a member of the PELS and the Brazilian Society of Power Electronics.

ADSON BEZERRA MOREIRA received the B.Sc. and M.Sc. degrees in electrical engineering from the Federal University of Ceará (UFC), Fortaleza, in 2003 and 2006, respectively, and the Ph.D. degree in electrical engineering from the State University of Campinas, Campinas, Brazil, in 2017. Since 2008, he has been with UFC/Sobral, Sobral, Brazil, where he is currently an Assistant Professor. His research interests include energy efficiency, power quality, electric machine drives, and power generation.

ERNESTO RUPPERT FILHO received the B.S. degree in electrical engineering and the M.S. and Ph.D. degrees from the University of Campinas (UNICAMP), Campinas, Brazil, in 1971, 1974, and 1983, respectively. From 1972 to 1978, he was with the Electrical and Computer Engineering School, UNICAMP, as an Assistant Professor of electromechanical energy conversion. From 1979 to 1983, he was with General Electric, Brazil, as an Application Engineer dedicated to large motors and generators and designing large induction and synchronous motors. From 1983 to 1989, he was with Vigesa Heavy Equipment, Brazil, where he was involved in designing very large hydrogenerators and also performing commissioning tests on hydropower plants in Brazil. He is currently a Full Professor with the Electrical and Computer Engineering School, UNICAMP, where he is involved in researching and teaching in the areas of electrical machines, power electronics, drives, and electrical power systems.